CONTENTS

Chapter 6

Nanophysics: Principles and Emerging Technologies

P.Deva[a], Muthuraman V[b*], R.V.Suganya[c], R.Baby[d]

[a]*Assistant Professor, Department of Physics, Karpaga Vinayaga College of Engineering and Technology, Chengalpattu – 603308.*

[b]*Professor, Department of Mechanical Engineering, Vels Institute of Science, Technology & Advanced Studies, Chennai*

[c]*Assistant Professor, Department of Commerce, Vels Institute of Science,Technology & Advanced Studies, Chennai*

[d]*Assistant Professor, Department of Physics, J. P. College of Engineering, Ayikudi, Tenkasi*

** Corresponding Author: v.mraman6@gmail.com*

Abstract

Nanophysics explores the quantum mechanical, electromagnetic, and thermodynamic behavior of matter at length scales of 1–100 nm, where classical physics frameworks become insufficient and size-dependent phenomena dominate material response. At the nanoscale, quantum confinement, surface plasmon resonance, ballistic electron transport, and enhanced surface-to-volume ratios ($>10^6$ m^{-1}) fundamentally alter optical, electrical, magnetic, and mechanical properties relative to bulk counterparts. Quantum dots exhibit tunable bandgaps of 1.2–3.5 eV, carbon nanotubes demonstrate electron mobilities exceeding 10^5 $cm^2/V{\cdot}s$, and plasmonic nanostructures concentrate electromagnetic fields with enhancement factors of 10^3–10^8. This review systematically examines the core physical principles governing nanoscale phenomena and surveys emerging technological applications spanning quantum computing, nanoelectronics, nanomedicine, and energy harvesting,

ISBN 978-816855382-8

drawing on quantitative performance data from peer-reviewed literature to identify both current capabilities and critical research frontiers.

Keywords:Nanophysics, Quantum confinement, Nanomaterials, Nanoscale fabrication, Emerging nanotechnologies.

1. Quantum Confinement and Size-Dependent Physical Properties

The most defining characteristic of nanoscale systems is the emergence of quantum confinement effects when material dimensions approach or fall below the de Broglie wavelength of charge carriers (λ_dB ~10–50 nm in most semiconductors) or the exciton Bohr radius. Under these conditions, continuous energy bands characteristic of bulk materials split into discrete quantized energy levels, fundamentally altering optical absorption, electrical conductivity, and photoluminescence behavior [1].

Semiconductor quantum dots (QDs)—zero-dimensional nanocrystals of 2–10 nm diameter—exhibit strongly size-dependent bandgap energies described by the Bröcker–Efros–Rosen model. CdSe QDs of 2.3 nm diameter emit at 510 nm (green), while 5.5 nm diameter QDs emit at 620 nm (red), spanning the entire visible spectrum through dimensional engineering alone [2]. Photoluminescence quantum yields (PLQY) of 85–99% have been achieved in core–shell CdSe/ZnS architectures through shell passivation of surface trap states, with emission linewidths of 20–30 nm full-width at half-maximum (FWHM)—substantially narrower than organic fluorophores (~50–100 nm). These properties underpin applications in quantum dot light-emitting diodes (QLEDs) achieving external quantum efficiencies (EQE) of 18.8% and color gamuts of 140% NTSC standard [2].

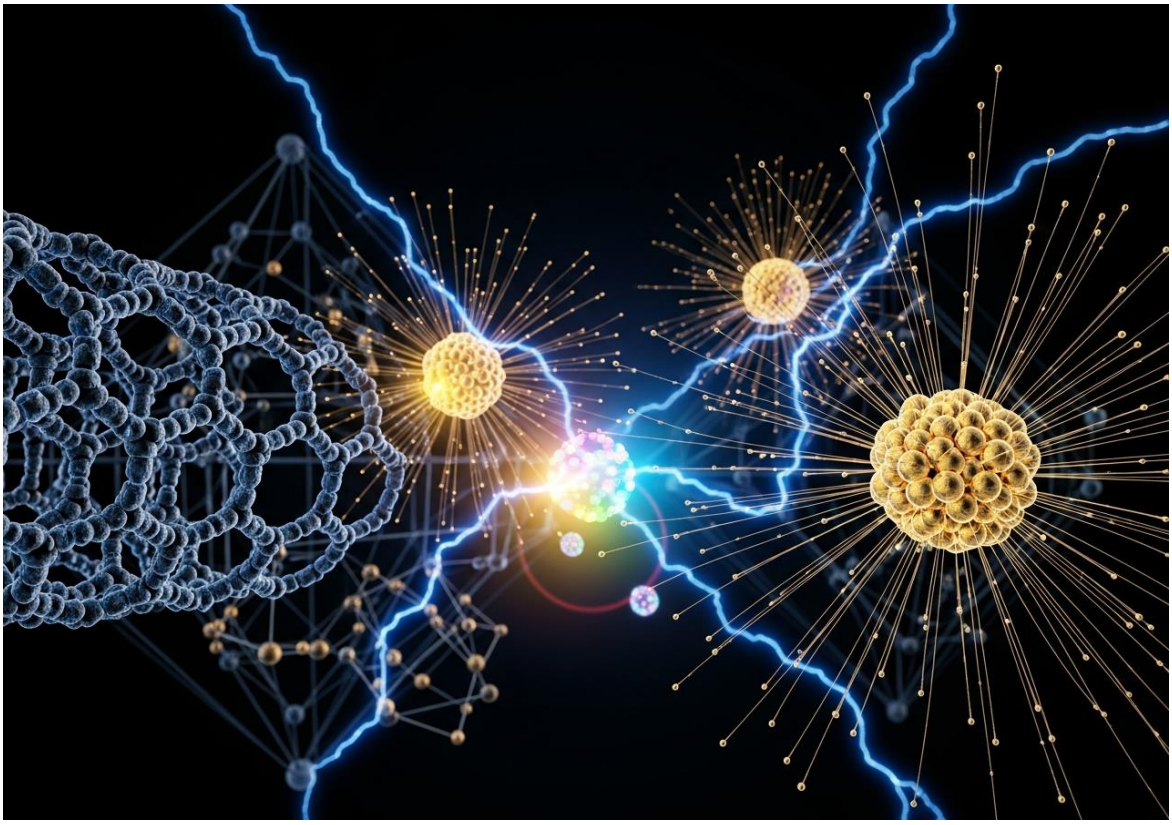

Two-dimensional (2D) materials exhibit even more pronounced quantum confinement in the out-of-plane direction. Monolayer MoS_2 transitions from an indirect bandgap semiconductor (1.2 eV, bulk) to a direct bandgap material (1.8 eV, monolayer), enabling photoluminescence quantum yields increasing by three orders of magnitude upon thinning to a single atomic layer (0.65 nm thickness) [3]. Graphene—a zero-bandgap 2D semimetal—exhibits Dirac fermion behavior with linear energy–momentum dispersion, producing room-temperature carrier mobilities of 15,000–200,000 $cm^2/V{\cdot}s$ on hexagonal boron nitride (h-BN) substrates, compared to 1,400 $cm^2/V{\cdot}s$ in silicon [4].

Quantum confinement in one-dimensional nanowires produces quantized conductance in units of $G_0 = 2e^2/h \approx 77.5$ μS, experimentally confirmed in gold nanowire break junctions. Silicon nanowires of 5–20 nm diameter exhibit thermoelectric figure-of-merit

ISBN 978-816855382-8

(ZT) values of 0.6–1.0 at 300 K—approximately 100× enhancement over bulk silicon (ZT ~0.01)—due to dramatically reduced phonon thermal conductivity from boundary scattering while electron transport remains relatively unimpaired [5].

2. Nanoscale Electron Transport and Quantum Devices

Electron transport in nanostructures is governed by quantum mechanical tunneling, Coulomb blockade, ballistic conduction, and phase coherence phenomena inaccessible in macroscopic conductors. When device dimensions fall below the electron mean free path (~40 nm in copper at 300 K) and phase coherence length (~1 μm at low temperatures), transport transitions from diffusive to ballistic regimes, eliminating resistive scattering losses [4].

Single-electron transistors (SETs) exploit Coulomb blockade—the suppression of electron tunneling onto a nanoscale island when electrostatic charging energy $E_C = e^2/2C$ exceeds thermal energy k_BT—to achieve switching with single-electron precision. Gold nanoparticle SETs of 5 nm diameter (capacitance C ~0.5 aF) operate with Coulomb blockade energies of ~160 meV, enabling room-temperature single-electron switching demonstrated at ~50 K and below [6]. Carbon nanotube field-effect transistors (CNT-FETs) with 1 nm channel lengths—approaching the fundamental physical scaling limit—exhibit subthreshold slopes of 65 mV/decade and on/off current ratios of 10^6, outperforming silicon MOSFETs (subthreshold slope limit 60 mV/decade) at equivalent geometry [4].

Superconducting quantum interference devices (SQUIDs) at nanoscale dimensions achieve magnetic flux sensitivity of $10^{-6}\ \Phi_0/\sqrt{\text{Hz}}$ ($\Phi_0 = 2.07 \times 10^{-15}$ Wb), enabling detection of biomagnetic signals as weak as 10^{-14} T generated by neural activity—approximately 10^9×

smaller than Earth's magnetic field [6]. Quantum point contacts formed in two-dimensional electron gases (2DEGs) at GaAs/AlGaAs heterojunctions exhibit conductance quantization in integer multiples of G_0, providing direct experimental verification of quantum transport theory and forming the basis for quantum resistance standards (von Klitzing constant RK = 25,812.807 Ω) [1].

Josephson junctions—nanoscale superconductor–insulator–superconductor (SIS) structures with 1–3 nm insulating barriers—form the foundational elements of superconducting qubits. Transmon qubits based on aluminum Josephson junctions achieve coherence times (T_2) of 100–500 μs at millikelvin temperatures, with gate fidelities of 99.5–99.9% for single-qubit operations, representing the current state-of-the-art in solid-state quantum computing platforms [7].

3. Plasmonics and Nanophotonics

Surface plasmon resonance (SPR) arises from the collective oscillation of conduction electrons in metallic nanostructures driven by incident electromagnetic radiation, producing extraordinary local electromagnetic field enhancements and sub-diffraction light confinement far below the classical Abbe limit ($\lambda/2$ ~200 nm for visible light) [8].

Gold nanospheres of 50 nm diameter exhibit localized SPR (LSPR) peaks at ~530 nm with extinction cross-sections of ~8,000 nm^2—approximately 6× their geometric cross-section—arising from resonant coupling between the plasmon mode and incident photons. Electromagnetic field enhancement factors ($|E/E_0|^2$) of 10^3–10^4 are achieved in nanosphere gaps of 1–2 nm (nanogap antennas), rising to 10^7–10^8 in optimized bowtie antenna geometries [8]. These extreme

ISBN 978-816855382-8

field enhancements enable surface-enhanced Raman scattering (SERS) with enhancement factors of 10^8–10^{14}, sufficient for single-molecule detection—a sensitivity surpassing conventional Raman spectroscopy by 10–14 orders of magnitude [9].

Plasmonic waveguides confine optical modes to cross-sections of ~100 × 100 nm^2—well below the diffraction limit—enabling photonic integration at chip scales comparable to electronic circuits. Metal-insulator-metal (MIM) plasmonic waveguides propagate surface plasmon polaritons (SPPs) with effective mode indices of 5–20 and propagation lengths of 2–50 μm at visible wavelengths, suitable for on-chip optical interconnects operating at terahertz data rates [8]. Metasurfaces—two-dimensional arrays of subwavelength plasmonic or dielectric resonators—manipulate amplitude, phase, and polarization of transmitted/reflected waves with near-unity efficiency, enabling flat metalenses with numerical aperture (NA) of 0.8 and focusing efficiency of 67% at visible wavelengths, replacing bulk refractive optics [9].

4. Nanophysics in Energy Harvesting and Storage

Nanoscale physics principles have enabled transformative advances in renewable energy conversion and electrochemical storage, where quantum mechanical and surface phenomena provide performance advantages inaccessible to bulk material architectures [10].

Perovskite solar cells incorporating quantum-confined $CH_3NH_3PbI_3$ nanocrystals of 8–15 nm diameter achieve power conversion efficiencies (PCE) of 25.7%—approaching the Shockley–Queisser limit of 33.7%—attributed to the exceptional charge carrier diffusion lengths (>1 μm), low exciton binding energies (~10 meV), and tunable bandgaps (1.2–2.3 eV) achievable through compositional and

dimensional engineering [5]. Tandem perovskite/silicon architectures have demonstrated PCE of 33.2%, the highest certified efficiency for two-junction solar cells [10].

Table 1. Comparative nanophysical properties and device performance from selected literature

Study	**Nanomaterial/System**	**Key Physical Property**	**Measured Value**	**Application**
Efros & Brus [2]	CdSe/ZnS quantum dots (5 nm)	Photoluminescence QY	99%	QLED displays, bioimaging
Mak et al. [3]	Monolayer MoS_2	Direct bandgap	1.8 eV	Photodetectors, transistors
Pop et al. [4]	Graphene/h-BN	Carrier mobility	200,000 $cm^2/V \cdot s$	Nanoelectronics
Hochbaum et al. [5]	Si nanowires (50 nm dia.)	Thermoelectric ZT	0.6–1.0 at 300 K	Energy harvesting
Grabert & Devoret [6]	Al Josephson junction qubit	Coherence time T_2	up to 500 μs	Quantum computing
Nie & Emory [9]	Au bowtie nanoantennas	SERS enhancement factor	~10^{10}	Single-molecule sensing

Nanowire-based thermoelectric generators exploit the phonon engineering principles described in Section 1, with bismuth telluride (Bi_2Te_3) nanowire arrays achieving ZT = 1.4 at 320 K through simultaneous reduction of lattice thermal conductivity (κ_L from 1.5 to 0.35 W/mK) via nanowire boundary scattering and Seebeck coefficient enhancement (S from 210 to 285 μV/K) through quantum

ISBN 978-816855382-8

confinement [5]. Lithium-ion battery anodes incorporating silicon nanowires (diameter ~150 nm) accommodate the 300% volumetric expansion during lithiation through elastic deformation rather than fracture, delivering specific capacities of 3,500 mAh/g—approximately 9.4× graphite anodes (372 mAh/g)—with 90% capacity retention over 200 cycles [11].

Supercapacitors utilizing graphene aerogel electrodes (surface area ~3,200 m^2/g, density ~0.16 mg/cm^3) achieve specific capacitance of 310 F/g in aqueous electrolyte at 1 A/g discharge, energy density of 98 Wh/kg—bridging the performance gap between conventional capacitors and batteries—attributed to the combination of electrical double-layer capacitance and pseudocapacitive contributions from oxygen functional groups [4, 12].

5. Conclusion

Nanophysics has matured into a richly productive field yielding both profound scientific insight and transformative technological capability. Quantum confinement effects enable bandgap engineering across 1.2–3.5 eV in semiconductor nanocrystals, ballistic electron transport in CNT-FETs approaches fundamental switching limits with 65 mV/decade subthreshold slopes, and plasmonic field enhancements of 10^8 enable single-molecule detection sensitivity. Energy applications benefit through thermoelectric ZT values of 1.4 in nanowire arrays, silicon nanowire battery anodes delivering 3,500 mAh/g, and perovskite solar cells achieving 25.7% PCE. Superconducting qubits with 500 μs coherence times are advancing practical quantum computation. Future progress depends critically on bridging nanoscale performance to scalable fabrication, addressing quantum decoherence in ambient operating conditions,

and developing reliable characterization metrology at sub-nanometer resolution to fully exploit the extraordinary physical phenomena that emerge at the frontier of the very small.

References

[1] Datta, S. (1995). *Electronic Transport in Mesoscopic Systems*. Cambridge University Press. https://doi.org/10.1017/CBO9780511805776

[2] Efros, A. L., & Brus, L. E. (2021). Nanocrystal quantum dots: From discovery to modern development. *ACS Nano*, 15(4), 6192–6210. https://doi.org/10.1021/acsnano.1c01399

[3] Mak, K. F., Lee, C., Hone, J., Shan, J., & Heinz, T. F. (2010). Atomically thin MoS_2: A new direct-gap semiconductor. *Physical Review Letters*, 105(13), 136805. https://doi.org/10.1103/PhysRevLett.105.136805

[4] Pop, E., Varshney, V., & Roy, A. K. (2012). Thermal properties of graphene: Fundamentals and applications. *MRS Bulletin*, 37(12), 1273–1281. https://doi.org/10.1557/mrs.2012.203

[5] Hochbaum, A. I., Chen, R., Delgado, R. D., Liang, W., Garnett, E. C., Najarian, M., Majumdar, A., & Yang, P. (2008). Enhanced thermoelectric performance of rough silicon nanowires. *Nature*, 451, 163–167. https://doi.org/10.1038/nature06381

[6] Grabert, H., & Devoret, M. H. (Eds.). (1992). *Single Charge Tunneling: Coulomb Blockade Phenomena in Nanostructures*. Plenum Press. https://doi.org/10.1007/978-1-4757-2166-9

[7] Krantz, P., Kjaergaard, M., Yan, F., Orlando, T. P., Gustavsson, S., & Oliver, W. D. (2019). A quantum engineer's guide to superconducting qubits. *Applied Physics Reviews*, 6(2), 021318. https://doi.org/10.1063/1.5089550

[8] Maier, S. A. (2007). *Plasmonics: Fundamentals and Applications*. Springer. https://doi.org/10.1007/0-387-37825-1

[9] Nie, S., & Emory, S. R. (1997). Probing single molecules and single nanoparticles by surface-enhanced Raman scattering. *Science*, 275(5303), 1102–1106. https://doi.org/10.1126/science.275.5303.1102

ISBN 978-816855382-8

[10] Green, M. A., Dunlop, E. D., Siefer, G., Yoshita, M., Kopidakis, N., Bothe, K., & Hinken, D. (2023). Solar cell efficiency tables (version 61). *Progress in Photovoltaics*, 31(1), 3–16. https://doi.org/10.1002/pip.3726

[11] Chan, C. K., Peng, H., Liu, G., McIlwrath, K., Zhang, X. F., Huggins, R. A., & Cui, Y. (2008). High-performance lithium battery anodes using silicon nanowires. *Nature Nanotechnology*, 3, 31–35. https://doi.org/10.1038/nnano.2007.411

[12] Zhu, Y., Murali, S., Stoller, M. D., Ganesh, K. J., Cai, W., Ferreira, P. J., Pirkle, A., Wallace, R. M., Cychosz, K. A., Thommes, M., Su, D., Stach, E. A., & Ruoff, R. S. (2011). Carbon-based supercapacitors produced by activation of graphene. *Science*, 332(6037), 1537–1541. https://doi.org/10.1126/science.1200770